Evidence for a monoclinic M_A to tetragonal morphotropic phase transition in $(1-x)[Pb(Fe_{1/2}Nb_{1/2})O_3]-xPbTiO_3$ ceramics

2007 J. Phys.: Condens. Matter 19 036217

(http://iopscience.iop.org/0953-8984/19/3/036217)

INSTITUTE OF PHYSICS PUBLISHING JOURNAL OF PHYSICS: CONDENSED MATTER

J. Phys.: Condens. Matter **19** (2007) 036217 (9pp) doi:10.1088/0953-8984/19/3/036217

Evidence for a monoclinic M_A to tetragonal morphotropic phase transition in $(1-x)[Pb(Fe_{1/2}Nb_{1/2})O_3]$–$xPbTiO_3$ ceramics

Satendra Pal Singh, Akhilesh Kumar Singh and Dhananjai Pandey

School of Materials Science and Technology, Institute of Technology, Banaras Hindu University, Varanasi-221 005, India

Received 4 May 2006, in final form 8 November 2006
Published 5 January 2007
Online at stacks.iop.org/JPhysCM/19/036217

Abstract

The results of a powder x-ray diffraction study of the evolution of the crystal structure in pyrochlore-free single-phase powders of $(1-x)[Pb(Fe_{1/2}Nb_{1/2})]O_3$–$xPbTiO_3$ (PFN–xPT) are presented. Rietveld analysis of the powder diffraction data reveals that the morphotropic phase transition in PFN–xPT corresponds to a change of structure from M_A-type monoclinic with Cm space group to tetragonal with $P4mm$ space group at $0.06 < x < 0.08$. It is argued that this monoclinic phase persists in the entire composition range $0.0 \leqslant x \leqslant 0.06$, as evidenced by the presence of anomalous broadening of the 200 profile. The similarity of the morphotropic phase boundary (MPB) in PFN–xPT with that in the $Pb(Zr_xTi_{1-x})O_3$ (PZT) is pointed out.

1. Introduction

Lead iron niobate $Pb(Fe_{1/2}Nb_{1/2})O_3$ (PFN) belongs to the family of lead-based complex perovskite compounds [1]. It is an attractive material for use in multilayer ceramic capacitors and other electronic devices due to its high dielectric constant (>10 000), diffuse phase transition behaviour and low sintering temperature [2]. PFN is a magnetoelectric undergoing a paraelectric to ferroelectric and a paramagnetic to antiferromagnetic phase transition at 385 K [1] and 143 K [3, 4], respectively. Further, the solid solution of PFN with $PbTiO_3$, i.e. $(1-x)[Pb(Fe_{1/2}Nb_{1/2})O_3]$–$xPbTiO_3$ (PFN–xPT), exhibits a morphotropic phase transition [5] similar to that in the well known piezoelectric ceramics $Pb(Zr_xTi_{(1-x)})O_3$ (PZT), $(1-x)[Pb(Mg_{1/3}Nb_{2/3})O_3]$–$xPbTiO_3$ (PMN–xPT), and $(1-x)[Pb(Zn_{1/3}Nb_{2/3})O_3]$–$xPbTiO_3$ (PZN–xPT) and $(1-x)[Pb(Sc_{1/2}Nb_{1/2})O_3]$–$xPbTiO_3$ (PSN–xPT) [6]. The morphotropic phase transition is of special technological interest since the dielectric and piezoelectric responses are known to be maximized near the morphotropic phase boundary (MPB) composition [7]. The MPB has generally been believed to separate the tetragonal and rhombohedral phase fields [6]. Recently, it has been shown that the tetragonal and rhombohedral phase fields are separated by a thin region of stability of one monoclinic phase

(M_A) in the MPB region of PZT [8, 9] and two (M_B and M_C) in the PMN–xPT [10] and PSN–xPT [11] ceramics. The high piezoelectric response of these ceramics has been attributed to the presence of these monoclinic phases which are believed to facilitate the rotation of the polarization vector from the [111] direction of the rhombohedral phase to the [001] direction of the tetragonal phase, as predicted theoretically [12, 13] and observed experimentally [14]. First-principles calculations have also confirmed the stability of a monoclinic phase in the MPB region of PZT [15]. We present here the first experimental evidence for a morphotropic phase transition from a monoclinic phase of M_A type with Cm space group to a tetragonal phase with $P4mm$ space group in the PFN–xPT system for $0.06 < x < 0.08$.

2. Experimental details

PFN–xPT ceramics prepared by solid-state route generally contain a small amount of an unwanted pyrochlore phase [16]. We have synthesized pyrochlore-phase-free PFN–xPT ceramics using a modified wolframite precursor method, the details of which are given elsewhere [17]. Analytic reagent grade chemicals, Fe_2O_3, Nb_2O_5, $PbCO_3$, and TiO_2, with minimum assay of 99% or more, were used to synthesize PFN–xPT. The various ingredients were ball milled in a planetary ball mill (Restch GmbH & Rheinische, Germany) using zirconia jars and zirconia balls with AR grade acetone as the mixing media. A wolframite precursor $FeNbO_4$ was first prepared by calcining a mixture of Fe_2O_3 and Nb_2O_5 at 1050 °C for 6 h. A slight excess (4 wt%) of Fe_2O_3 was used to prevent the formation of the pyrochlore phase. TiO_2 powder was subsequently mixed with $FeNbO_4$ and the mixture was calcined at 1050 °C for another 6 h to obtain $[(1 - x)/2FeNbO_4–xTiO_2]$ (FNT) precursor. This FNT precursor was finally mixed with $PbCO_3$ and calcined at 800 °C for 6 h in air. The calcined powder was pelletized using a steel die of 12 mm diameter in a uniaxial hydraulic press at an optimized load of 65 kN. A 2% polyvinyl alcohol (PVA) solution in water was used as a binder. The green pellets were kept at 500 °C for 10 h to burn off the binder material and then sintered at 1150 °C for 6 h in a sealed alumina crucible with controlled PbO atmosphere. The density of the sintered pellets was higher than 98% of the theoretical value. For x-ray characterization, the sintered pellets were crushed to fine powders and then annealed at 500 °C for 10 h to remove the strains introduced during crushing. X-ray diffraction (XRD) measurements were carried out using an 18 kW rotating anode (Cu) based Rigaku powder diffractometer operating in the Bragg–Brentano geometry and fitted with a graphite monochromator in the diffracted beam. The data were collected in the 2θ range 20°–120° with a step of 0.02°.

3. Results and discussion

In the PFN–xPT ceramics, the location of the MPB is controversial. According to early reports [5], the MPB is located around $x = 0.05 < x < 0.06$, while in recent years it has been claimed to be between $x = 0.10$ and 0.20 [18]. In thin films of PFN–xPT prepared by the sol–gel route, the MPB has been claimed to lie around $x = 0.50$ [19]. Our preliminary work [20] has revealed that the MPB is located in the range $0 < x < 0.10$.

In order to locate the MPB region in the PFN–xPT ceramics precisely, we have analysed the powder x-ray diffraction profiles of the 200, 220, and 222 pseudocubic reflections for various compositions in the range $0 < x < 0.10$ (see figure 1). For the tetragonal phase, the 200 pseudocubic reflection is a doublet while 222 a singlet, whereas for the rhombohedral phase 200 is a singlet and 222 a doublet. The 220 reflection is, on the other hand, a doublet for both the tetragonal and rhombohedral structures but the stronger 202 peak occurs on the lower 2θ side of the weaker 220 for tetragonal phase, whereas the stronger $2\bar{2}0$ peak of the

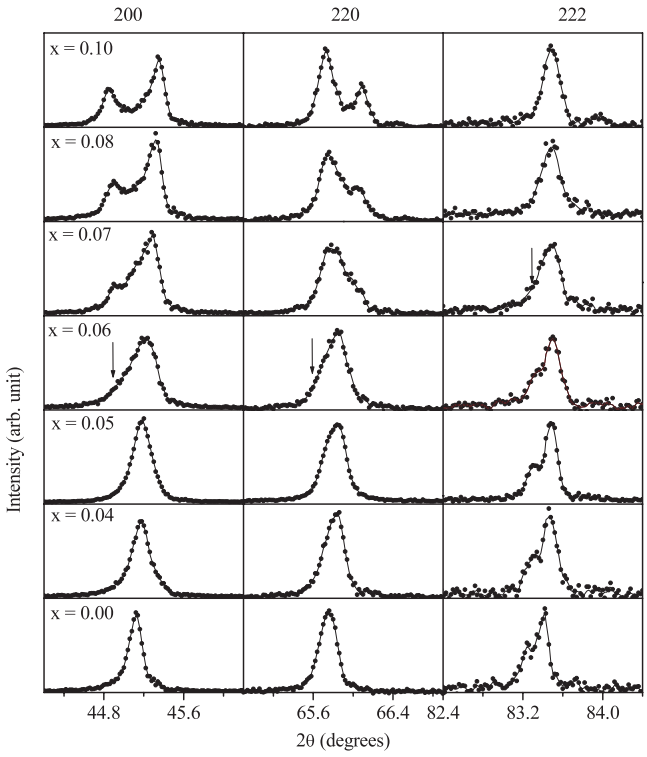

Figure 1. The 200, 220 and 222 pseudocubic x-ray diffraction profiles for $(1-x)[Pb(Fe_{1/2}Nb_{1/2})]O_3$–$xPbTiO_3$ ceramics with $x = 0.0$, 0.04, 0.05, 0.06, 0.07, 0.08 and 0.10. The Cu Kα_2 contribution has been removed in all the profiles using software. The dots represent the observed data points while the continuous lines represent the smoothened plots.

rhombohedral phase occurs on the higher 2θ side of the weaker 220 peak. It can be seen from figure 1 that for pure PFN (i.e. for $x = 0.00$), 200 is a singlet while 222 is a doublet. The large broadening of the 220 profile indicates that it is also not a singlet. Thus the structure of PFN is only 'apparently' rhombohedral. With increasing PT content, the structure eventually becomes tetragonal for $x \geqslant 0.08$ as 200 and 220 are now doublets while 222 has become a singlet. For $x = 0.06$, the 222 is although a doublet, the 200 and 220 profiles do not correspond to singlet peak as can be inferred from the large asymmetric broadening on the lower 2θ side of these profiles, as shown with arrow marks in figure 1. On increasing the PT content further to $x = 0.07$, the splitting of the 200 peak is clearly observed but the 222 peak no longer exhibits splitting. However, the latter is not a singlet since it exhibits a large asymmetric broadening on the lower 2θ side. The 220 peak, on the other hand, continues to exhibit large broadening which is, unlike for $x = 0.06$, more pronounced on the higher 2θ side. All these features of the diffraction profiles for $x = 0.06$ and 0.07 cannot be attributed to a pure tetragonal or a pure rhombohedral structure but can arise due to a coexistence of the tetragonal and rhombohedral phases or due to the presence of a monoclinic phase [9]. The eighth-order Landau theory [13] for ferroelectric transitions in perovskites predicts three monoclinic phases of M_A, M_B and M_C types with Cm, Cm and Pm space groups, respectively. Vanderbilt and Cohen distinguish between M_A and M_B types for the Cm space group on the basis of the values of polarization components, **Px**, **Py** and **Pz**, along the pseudocubic axes. For the M_A phase, which is observed in the PZT ceramics [8, 9, 21], $\mathbf{Px} = \mathbf{Py} < \mathbf{Pz}$, whereas for the M_B phase, which is observed in

PMN–xPT [10] and PSN–xPT [11] ceramics, $\mathbf{Px} = \mathbf{Py} > \mathbf{Pz}$. This implies that the equivalent pseudocubic cell parameters will bear the following relationships: $a_m/\sqrt{2} \approx b_m/\sqrt{2} < c_m$ for M_A and $a_m/\sqrt{2} \approx b_m/\sqrt{2} > c_m$ for M_B phase [22]. The M_C type monoclinic phase with space group Pm is observed in PMN–xPT [10, 23] and PSN–xPT system [11].

In view of the foregoing, we considered the following structural models for describing the powder XRD pattern of PFN–xPT with $x = 0.06$: (i) a mixture of rhombohedral (space group $R3m$) and tetragonal (space group $P4mm$) phases, (ii) a pure monoclinic phase with space group Pm, and (iii) a pure monoclinic phase with space group Cm. In order to make a choice between these three models, Rietveld refinements were carried out using the FullProf program [24]. For the sake of comparison with pure PFN, we also refined the structure for $x = 0.06$ using the $R3m$ space group. In the refinements, a pseudo-Voigt function and a sixth-order polynomial were used to define the profile shape and the background, respectively. Except for the occupancy parameters of the ions, which were fixed at the nominal composition, all other parameters, such as scale factor, zero correction, background, half-width parameters, the mixing parameters, lattice parameters, positional coordinates, and thermal parameters, were varied in the course of refinement using isotropic and anisotropic peak broadening functions. It was found necessary to consider anisotropic peak broadening functions [25] to get satisfactory fits between observed and calculated profiles. The refined isotropic thermal parameter for Pb was found to be very large (∼2.8), indicating Pb-site disorder, similar to that reported in pure PFN [26]. Following previous workers [26], we therefore used anisotropic thermal parameters in our refinements, which resulted in lower χ^2 values and acceptable thermal parameters. The refinement converged smoothly after a few cycles for all the structural models.

In the tetragonal phase with $P4mm$ space group, there are four ions in the asymmetric unit with the Pb^{2+} ion in 1(a) sites at $(0, 0, z)$, $Ti^{4+}/Nb^{5+}/Fe^{3+}$ and O_I^{2-} in 1(b) sites at $(1/2, 1/2, z)$ and O_{II}^{2-} in 2(c) sites at $(1/2, 0, z)$. For the rhombohedral phase with $R3m$ space group, we have used hexagonal axes with lattice parameters $a_H = b_H = \sqrt{2}a_R$ and $c_H = \sqrt{3}a_R$, where a_R corresponds to the rhombohedral cell parameter. There are three ions in the asymmetric unit of the rhombohedral structure, Pb^{2+} and $Nb^{5+}/Ti^{4+}/Fe^{3+}$ ions in 3(a) sites at $(0, 0, z)$ and O^{2-} ions in 9(b) sites at $(2x, x, 1/6)$. In the monoclinic phase with space group Cm, there are four ions in the asymmetric unit with Pb^{2+}, $Ti^{4+}/Nb^{5+}/Fe^{3+}$, and O_I^{2-} in 2(a) sites at $(x, 0, z)$ and O_{II}^{2-} in 4(b) sites at (x, y, z). The asymmetric unit cell of the monoclinic phase with space group Pm has five ions, with Pb^{2+} and O_I^{2-} in 1(a) sites at $(x, 0, z)$, $Ti^{4+}/Nb^{5+}/Fe^{3+}$, O_{II}^{2-}, and O_{III}^{2-} in 1(b) sites at $(x, 1/2, z)$. Pb^{2+} was fixed at origin $(0, 0, 0)$ in the tetragonal and monoclinic phases.

Figure 2 compares the observed, calculated and difference profiles of the pseudocubic 200, 220 and 222 peaks for the four models mentioned above for $x = 0.06$. The vertical 'tick' marks above the difference profile show the positions of various reflections for Cu Kα_1 and Cu Kα_2 radiation. It is evident from figure 2(a) that the mismatch between the observed and calculated profiles is quite prominent for all the three reflections for the $R3m$ space group. This is also indicated by the largest value of $\chi^2 = 2.77$ for this space group. Thus the $R3m$ space group is clearly ruled out. We also considered an orthorhombic structure with $Bmm2$ space group as a possibility but it could not account for the peak positions in the observed diffraction pattern (e.g. splitting of the 222 peak in figure 2). Consideration of $R3m$ and $P4mm$ coexistence, pure Pm and pure Cm models gives χ^2 values of 2.17, 1.94 and 1.79, respectively. The corresponding numbers of refinable structural parameters for these three models are 18, 17 and 15, respectively. The fact that the Cm space group with the lowest number (15) of refinable structural parameters gives the lowest χ^2 value clearly favours the Cm space group. This was further confirmed using Prince's [27] criterion. Here, one first calculates the functions x_i and z_i from the calculated intensities $M_1(S_i)$ and $M_2(S_i)$ and the observed intensity y_i at point S_i for

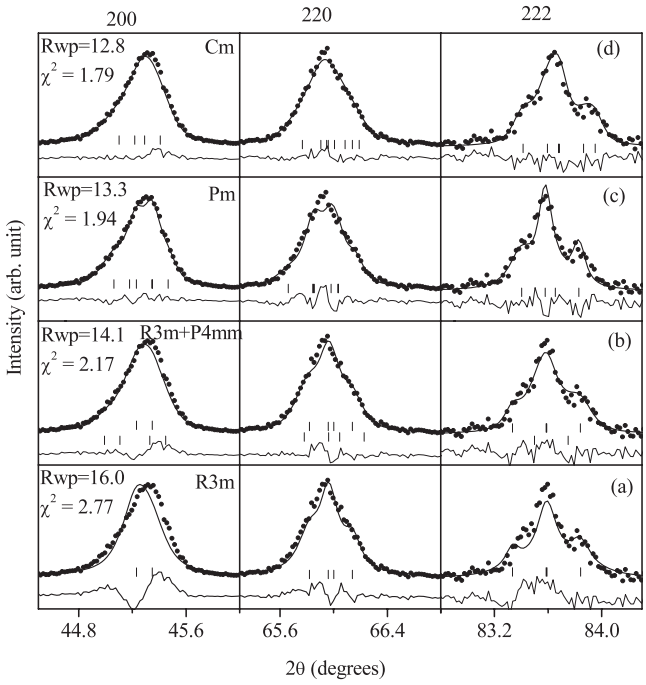

Figure 2. Observed (dots), calculated (continuous line), and difference (bottom line) profiles of the 200, 220 and 222 pseudocubic reflections obtained from the Rietveld analysis of the powder XRD data of $0.94Pb(Fe_{1/2}Nb_{1/2})O_3$–$0.06PbTiO_3$ in the 2θ range 20°–120° using different structural models. The tick marks above the difference plot show the positions of the Bragg peaks.

the two models M_1 and M_2 being compared (i.e. comparison of the coexistence of $R3m$ and $P4mm$ with pure Cm, or comparison of Pm with Cm in the present case):

$$x_i = \frac{[M_1(S_i) - M_2(S_i)]}{y_i^{1/2}}, \tag{1}$$

$$z_i = \frac{[y_i - (1/2)\{M_1(S_i) + M_2(S_i)\}]}{y_i^{1/2}}. \tag{2}$$

Then the slope η of the regression line $z_i = \eta x_i$ which minimizes $f(\eta) = \sum_{i=1}^{n} (z_i - \eta x_i)^2$ is obtained:

$$\eta = \frac{\sum_{i=1}^{n} z_i x_i}{\sum_{i=1}^{n} x_i^2}. \tag{3}$$

This slope η was found to be $-0.461\,96$ and $-0.282\,08$ respectively for comparison of the coexistence of $R3m$ and $P4mm$ with pure Cm, on one hand, and Pm with Cm on the other. A negative value of η implies that model M_2 gives a better fit to the observed data. Here we have chosen model M_2 for the Cm space group in both cases. Hence, Cm is obviously the preferred model as compared to the coexistence of $R3m$ and $P4mm$ model, or the Pm model. The Cm space group also gives a satisfactory overall fit between the observed and calculated profiles, as shown in figure 3 for the 2θ range 20°–120°. Table 1 lists the refined structural parameters for the monoclinic Cm space group. The cell parameters of the monoclinic Cm phase given in table 1 bear the relationship $a_m/\sqrt{2} \approx b_m/\sqrt{2} < c_m$ and hence this phase is of M_A type in the sense of Vanderbilt and Cohen [13]. The calculated bond lengths using the

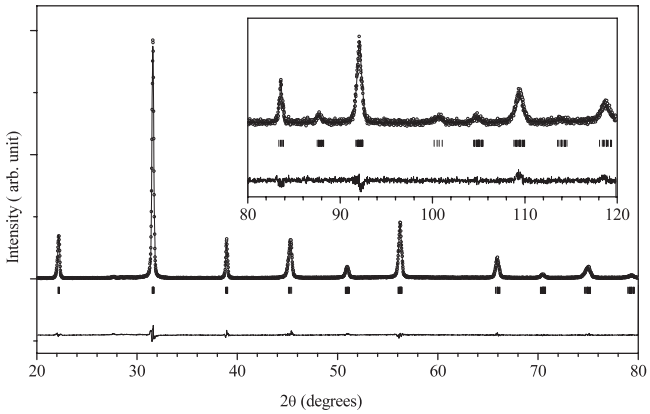

Figure 3. Part of the observed (dots), calculated (continuous line), and difference (bottom line) profiles obtained from the Rietveld analysis of $0.94Pb(Fe_{1/2}Nb_{1/2})O_3$–$0.06PbTiO_3$ using a monoclinic structure with *Cm* space group. The remaining part (80°–120°) is shown in the inset.

Table 1. Refined structural parameters of $0.94Pb(Fe_{1/2}Nb_{1/2})O_3$–$0.06PbTiO_3$ for a monoclinic structure with *Cm* space group.

$a = 5.6603(3)$ Å; $b = 5.6565(4)$ Å; $c = 4.0171(1)$ Å; $\alpha = \gamma = 90.00$ and $\beta = 90.149(4)°$				
Ions	x	y	z	B (Å^2)
Pb^{2+}	0.0000	0.0000	0.0000	$\beta_{11} = 0.025(3)$ $\beta_{22} = 0.027(3)$ $\beta_{33} = 0.027(2)$ $\beta_{13} = 0.002(2)$
$Ti^{4+}/Fe^{3+}/Nb^{5+}$	0.500(3)	0.0000	0.465(9)	$B = 0.66(4)$
O_I^{2-}	0.554(8)	0.0000	−0.03(1)	$B = 0.6(3)$
O_{II}^{2-}	0.274(9)	0.257(7)	0.429(5)	$B = 0.4(2)$
$R_p = 8.97$; $R_{wp} = 12.8$; $R_{\exp} = 9.55$; $\chi^2 = 1.79$				

program Bond_STR and its GUI Gbond_Str (version March 2005, J Rodriguez-Carvajal-LLB) in the FullProf program [24] for the *Cm* model are listed in table 2. Bond lengths listed in table 2 are comparable to those reported by Lampis *et al* [26] for pure PFN. The largest and the smallest Pb–O bond lengths listed in table 2 are also in excellent agreement with the upper and lower bounds for the bond lengths (3.20 and 2.53 Å) in the tetragonal phase of $PbTiO_3$, reported by Shirane *et al* [28].

Our Rietveld refinements thus show that there is a monoclinic phase with *Cm* space group of M_A type in the PFN–*x*PT system for $x = 0.06$. As said earlier, on increasing the PT content the structure changes to tetragonal for $x \geqslant 0.08$, which implies that the morphotropic phase transition in PFN–*x*PT occurs at $0.06 < x < 0.08$, in agreement with the earlier report of Berlincourt [5]. This disproves the claims of other workers for the MPB to lie in the composition range $x = 0.10 < x < 0.20$ [18] or at $x = 0.50$ [19]. It is worth mentioning here that in PZT [8, 9] and PMN–*x*PT [10, 23] ceramics, a small amount of tetragonal phase coexists with the monoclinic phase in the MPB region. A similar possibility of coexistence of tetragonal phase with the monoclinic phase in the PFN–*x*PT ceramics also cannot be ruled out. However, this can only be resolved using higher-resolution synchrotron XRD data.

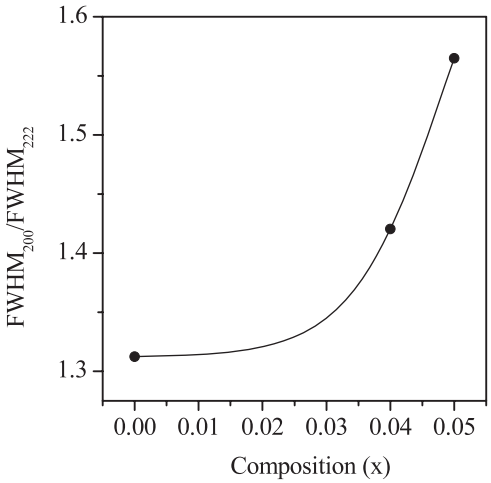

Figure 4. Ratio of the FWHM of the 200 reflection to that of the 222 reflection as a function of x for PFN–xPT ceramics with $0.0 \leqslant x \leqslant 0.05$.

Table 2. Bond lengths (Å) for the Cm space group.

$Pb–O_I$	$2.53(5) \times 1$
	$3.14(5) \times 1$
	$2.847(5) \times 2$
$Pb–O_{II}$	$3.13(3) \times 2$
	$2.73(4) \times 2$
	$2.96(3) \times 2$
	$2.55(4) \times 2$
$Fe/Nb/Ti–O_I$	$2.01(5) \times 1$
	$2.05(5) \times 1$
$Fe/Nb/Ti–O_{II}$	$1.94(5) \times 2$
	$2.08(5) \times 2$
$O_I–O_{II}$	$3.05(5) \times 2$
	$2.84(5) \times 2$
	$2.86(5) \times 2$
	$2.61(5) \times 2$
$O_{II}–O_{II}$	$2.91(6) \times 1$
	$2.75(6) \times 1$
	$2.83(7) \times 2$

Having found evidence for a monoclinic phase for $x = 0.06$, the next pertinent issue is to determine the stability of this phase for $x < 0.06$. For compositions with $0 \leqslant x \leqslant 0.05$, the pseudocubic 200 reflection appears to be a singlet while 222 is a well split doublet, suggesting the structure to be rhombohedral for these compositions. However, the width of the 200 peak is significantly larger than the width of $222/22\bar{2}$ for all compositions up to $x = 0.00$. Ideally, the $222/22\bar{2}$ reflection should be broader than the 200 peak following the Caglioti relationship [29] for the 2θ dependence of the full width at half maximum (FWHM). Figure 4 gives the variation of the ratio of the width of the 200 peak to that of the 222 as a function of x. It is evident from this figure that this ratio, which should have been less than 1.0, is invariably larger than 1 even

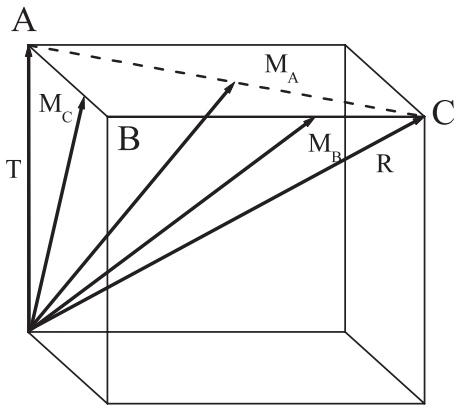

Figure 5. Polarization rotation paths involving various monoclinic phases (after [10, 12]).

for $x = 0.00$. It has been shown by Ragini *et al* [9] in PZT and Singh and Pandey [10, 22] and Singh *et al* [30] in PMN–xPT that this anomalous broadening arises due to short-range ordered domains of the monoclinic Cm phase. This idea has been further developed by Glazer *et al* [31], who have argued that the short-range monoclinic ordering in the pseudorhombohedral compositions of PZT becomes long-range ordered monoclinic phase near the MPB of PZT followed by short-range monoclinic ordering in the pseudotetragonal compositions on the other side of the MPB. We believe that the anomalous broadening of the 200 peak, present only in the apparently rhombohedral compositions ($x < 0.06$) of PFN–xPT, and not in the tetragonal compositions, which is similar to that in PZT [9, 21] and PMN–xPT [10, 22, 30], is due to the short-range ordered monoclinic regions for $x < 0.06$. In fact, Lampis *et al* [26] had proposed Cm space group for pure PFN ($x = 0.00$) below 355 K on the basis of a Rietveld analysis of powder x-ray and neutron diffraction data. The results presented in the present work suggest that the short-range ordered monoclinic regions in pure PFN grow on increasing the PT content until it becomes a full blown monoclinic phase for $x = 0.06$.

It is interesting to note that the M_A to tetragonal morphotropic phase transition in PFN–xPT is similar to that in the PZT system but quite different from that of the relaxor ferroelectric-based MPB systems [10, 11, 22]. The polarization rotation paths for PFN–xPT and PZT, on the one hand, and PMN–xPT and PSN–xPT on the other, are quite different. Following Fu and Cohen [12] and Vanderbilt and Cohen [13], the polarization vector of the tetragonal phase in the [001] direction can rotate in the (110) plane as shown by the line AC in figure 5 in order to reach the point C corresponding to the polarization vector of the rhombohedral phase in the [111] direction. This is the situation for PZT and PFN–xPT even though for $x = 0.0$ the structure is only pseudorhombohedral for PFN–xPT. On the other hand, for the other MPB systems, like PMN–xPT and PSN–xPT, the complete polarization rotation from [001] to [111] occurs along the AB and BC directions in figure 5, which requires the existence of two monoclinic phases of M_C and M_B type, as was first shown experimentally in PMN–PT [10] and later on confirmed in PSN–PT [11] also. This leads to two peaks in the composition dependence of the dielectric constant [10] and piezoelectric coefficient [32] corresponding to two MPBs at the M_B–M_C and M_C–$P4mm$ phase boundaries. The space group symmetry becomes orthorhombic $Bmm2$ when the polarization vector is exactly at the point B in figure 5. The elastic energy minimization at M_A–$P4mm$, M_B–M_C and M_C–$P4mm$ favours the existence of such phase boundaries [33]. However, it is not clear why MPB systems based on one class of $A(B, B')O_3$ type complex perovskites, like PMN and PSN, show M_B and M_C type monoclinic phases while

those based on PFN exhibit the M_A type monoclinic phase. We hope that our observations will encourage first-principles total energy calculations in future to understand this difference. We believe that the magnetoelectric nature of PFN is responsible for this difference.

To summarize, we have presented evidence for a monoclinic M_A (space group Cm) to tetragonal (space group $P4mm$) morphotropic phase transition in the PFN–xPT system for $0.06 < x < 0.08$. This monoclinic phase is similar to that observed in the PZT system but different from the M_C and M_B type monoclinic phases reported in the other complex perovskite-based MPB systems, like PMN–xPT and PSN–xPT. This is the first example of a monoclinic to tetragonal morphotropic phase transition in a mixed system, one of whose end members (PFN) is a magnetoelectric.

Acknowledgment

Satendra Pal Singh acknowledges financial support from the All India Council of Technical Education (AICTE) in the form of the award of a National Doctoral Fellowship (NDF).

References

[1] Smolenskii G A, Agranovskia A I, Popov S N and Isupov V A 1958 *Sov. Phys.—Tech. Phys.* **3** 1981
[2] Yonezawa M 1983 *Am. Ceram. Soc. Bull.* **62** 1375
[3] Bokov V A, Mylnikova I E and Smolenskii G A 1962 *Sov. Phys.—JETP* **15** 447
[4] Yang Y, Liu J M, Huang H B, Zou W Q, Bao P and Liu Z G 2004 *Phys. Rev.* B **70** 132101
[5] Berlincourt D 1960 *SC-4443 (RR) 1960 Sandia Corporation Technical Report* US Department of Commerce, Washington 25, DC
[6] Jaffe B, Cook W R and Jaffe H 1971 *Piezoelectric Ceramics* (London: Academic)
[7] Park S-E and Shrout T R 1997 *J. Appl. Phys.* **82** 1804
[8] Noheda B, Cox D E, Shirane G, Guo R, Jones B and Cross L E 2000 *Phys. Rev.* B **63** 014103
[9] Ragini, Ranjan R, Mishra S K and Pandey D 2002 *J. Appl. Phys.* **92** 3266
[10] Singh A K and Pandey D 2003 *Phys. Rev.* B **67** 064102
[11] Haumont R, Al-Barakaty A, Dkhil B, Kiat J M and Bellaiche L 2005 *Phys. Rev.* B **71** 104106
[12] Fu H and Cohen R E 2000 *Nature* **403** 281
[13] Vanderbilt D and Cohen M H 2001 *Phys. Rev.* B **63** 094108
[14] Guo R, Cross L E, Park S-E, Noheda B, Cox D E and Shirane G 2000 *Phys. Rev. Lett.* **84** 5423
Noheda B, Cox D E, Park S-E, Shirane G, Cross L E and Zhong Z 2001 *Phys. Rev. Lett.* **86** 3891
[15] Bellaiche L, Garcia A and Venderbilt D 2000 *Phys. Rev. Lett.* **84** 5427
[16] Jenhi M, El Ghadraoui E H, Bali H, El Aatmani M and Rafiq M 1998 *Eur. J. Solid State Inorg. Chem.* **3** 221
[17] Singh S P and Pandey D 2007 unpublished
[18] Sunder V V S S S and Umarji A M 1995 *Mater. Res. Bull.* **30** 427
[19] Hashimoto T, Ishibashi K and Yako T 1997 *J. Sol–Gel Sci. Technol.* **9** 211
[20] Singh S P, Singh A K, Pandey D, Sharma H and Parkash O 2003 *J. Mater. Res.* **18** 2677
[21] Noheda B, Gonzalo J A, Cross L E, Guo R, Park S-E, Cox D E and Shirane G 2000 *Phys. Rev.* B **61** 8687
[22] Singh A K and Pandey D 2005 *Ferroelectrics* **326** 91
[23] Noheda B, Cox D E, Shirane G, Gao J and Ye Z-G 2002 *Phys. Rev.* B **66** 054104
[24] Rodriguez J-C 2005 Laboratory Leon Brillouin (CEA-CNRS) CEA/Saclay, 91191 Gif sur Yvette Cedex, France Fullprof (version December 2005)
[25] Stephens P W 1999 *J. Appl. Crystallogr.* **32** 281
[26] Lampis N, Sciau P and Lehmann A G 1999 *J. Phys.: Condens. Matter* **11** 3489
[27] Young R A 1996 The Rietveld method *International Union of Crystallography* (New York: Oxford University Press) pp 52–4
[28] Shirane G, Ray P and Frazer B C 1956 *Acta Crystallogr.* **9** 131
[29] Caglioti G, Paeoletti A and Ricci F P 1958 *Nucl. Instrum.* **3** 223
[30] Singh A K, Pandey D and Zaharko O 2006 *J. Appl. Phys.* **99** 076105
[31] Glazer A M, Thomas P A, Baba-Kishi K Z, Pang G K H and Tai C W 2004 *Phys. Rev.* B **70** 184123
[32] Guo Y, Luo H, Ling D, Xu H, He T and Yin Z 2003 *J. Phys.: Condens. Matter* **15** L77
[33] Topolov V Y and Ye Z G 2004 *Phys. Rev.* B **70** 094113